Electronic Supplementary Material (ESI) for Biomaterials Science.
This journal is © The Royal Society of Chemistry 2019

Covalent Conjugation of Bioactive Peptides to Graphene Oxide for Biomedical Applications

Karoline E. Eckhart,[†] Brian D. Holt,[†] Michaela G. Laurencin,[‡] Stefanie A. Sydlik*[†]

[†]*Department of Chemistry, Carnegie Mellon University, Pittsburgh, PA, USA*
[‡]*Department of Electrical and Computer Engineering, Carnegie Mellon University, Pittsburgh, PA, USA*

Supplementary Information

Correspondence Address
Professor Stefanie A. Sydlik Department of Chemistry Carnegie Mellon University 4400 Fifth Avenue Pittsburgh, PA 15213, United States

Table of Contents

A. Instrumentation (Pages 3-5)
    a. Table S1: XPS Deconvolution Parameters (Page 4)
B. Calculations (Page 5)
    a. Scheme S1: Calculation of Pep-G Surface Coverage (Pages 5-6)
C. Material Characterization
    a. Figure S1: DLS of Graphenic Starting Materials (Page 6)
    b. Figure S2: Endcapping Control (Pages 6-7)
    c. Figure S3: GPC of Peptides (Page 8)
    d. Table S2: Molecular Weights of Peptides (Page 8)
    e. Figure S4: FTIR Spectroscopy (Page 9)
    f. Figure S5: TGA (Page 9)
    g. Figure S6: XPS Deconvolution of Deprotected Peptide-Graphene Conjugates (Page 10)
    h. Figure S7: XRD (Page 11)
    i. Figure S8: Bulk Properties of Covalent Pep-Gs (Page 12)
    j. Figure S9: Mechanical Properties of Noncovalent Pep+G Blend (Page 12)
D. Methods (Pages 13-16)
    a. Figure S10: Electrical Stimulation Experimental Set-up (Page 16)
E. References (Page 17)

A. Instrumentation

Nuclear Magnetic Resonance (NMR) Spectroscopy

A 500 MHz NMR (Bruker Avance™ 500) was used to acquire ^{1}H NMR spectra of unconjugated, protected peptides in dimethyl sulfoxide-d_6. End group analysis using Mestrenova software (version 12.0.1) was used to determine degree of polymerization, which allowed estimation of M_n.

Gel Permeation Chromatography (GPC)

Dispersity of protected (unconjugated) peptides was analyzed via size exclusion chromatography with dimethylformamide at 35˚C as eluent at a constant flow rate of 1.00 mL/min and differential refractive index (RI) detector (Waters and Wyatt).

Fourier Transform Infrared (FTIR) Spectroscopy

FTIR attenuated total reflectance spectroscopy was performed using a PerkinElmer Frontier FTIR spectrometer with a germanium crystal. Spectra were acquired with a 0.25 cm^{-1} resolution over a range of 700-4000 cm^{-1}. Using the Spectrum software (PerkinElmer), spectra were corrected for attenuated total reflectance mode, baseline corrected, converted to absorbance, and normalized to the consistent peak at 896 cm^{-1}.

Thermogravimetric Analysis (TGA)

TGA was performed using a PerkinElmer TGA 4000 with Pyris Software. Samples were run under nitrogen with a flow rate of 20 mL min^{-1}. Samples (4-6 mg) were heated from 50-800˚C at a rate of 10˚C min^{-1} and the mass was monitored with a step size of 0.17˚C. TRIOS software (TA Instruments) was used to calculate the onset of degradation temperature (T_{on}), offset of degradation temperature (T_{off}), and first derivative. The first derivative curve was used to calculate the peak of degradation temperature (T_p), and functional group weight loss.

X-Ray Photoelectron Spectroscopy (XPS)

Survey scans as well as high-resolution N1s, C1s, and O1s scans were performed on each material using a Thermo Fisher ESCALAB 250 Xi XPS (Thermo Fisher, Waltham, MA). Samples, affixed to a piece of double-sided copper tape, were irradiated with monochromatic aluminum Kα X-rays, charge compensation, and a 600 micron spot size. A minimum of 5 survey scans were performed for each material with a 1.00 eV step size and 150.0 eV pass energy. For O1s and N1s, a minimum of 10 scans were performed using a 0.1 eV step size and 50.0 eV pass energy. For N1s, raw data was smoothed using a house-made MATLAB code (Mathworks, Natick, MA). Peak fitting of high-resolution elemental scans was performed using a free deconvolution software, Fityk 0.9.8.[13] Using this software, high resolution N1s and O1s data was Shirley baseline corrected and fit with a series of Lorentzian peaks using the Levenberg-Marquardt method.

Table S1. Deconvolution peak parameters, such as peak center (binding energy) and width (full width at half max), can be defined using reference materials with known chemical compositions in addition to referencing literature for XPS deconvolution schemes of materials that are similar in chemical composition to the target analyte.[2] The following peak parameters were maintained in deconvolution of high resolution XPS spectra of graphenic materials:

Peak Identity	Peak Center	FWHM	Reference Material
Alcohol (-**O**H)	533.5 ± 0.1	2	Literature[3]
Carboxylic acid (O-C=**O**)	532.6 ± 0.1	2	H-Leu-OH
Oxygen in amide (N-C=**O**)	531.6 ± 0.1	2	p(Glu-Bzl)
C-**O**	530.9 ± 0.1	2	p(Glu-Bzl)
Ammonium (-**N**H_3)	402.6 ± 0.5	2	Literature[4]
Amine (-**N**H_2)	400.7 ± 0.1	2	H-Lys(Z)-OH, H-Leu-OH
Nitrogen in amide (**N**-C=O)	399.3 ± 0.1	1.6	p(Lys-Z)
Nitrogen in carbamate (**N**-C=O-O)	398.4 ± 0.1	1.6	H-Lys(Z)-OH

X-Ray Powder Diffraction (XRD)

XRD was conducted using an X'Pert powder diffractometer using Cu Kα radiation on a PIXcel detector (Malvern, Worcestershire, UK). The scan range was 5.005-19.99978 2θ with a step size of 0.105042 2θ.

Dynamic Light Scattering

GO and CG solutions, each with a concentration of 100 μg/mL in water, were briefly (~5 s) bath sonicated (240 W, 42 kHz, ultrasonic cleaner, Kendal) to disperse flocculants. A Zetasizer Nano ZS (Malvern Instruments Ltd., Worcestershire, UK) was used to perform DLS using Zetasizer Software v7.12 (Malvern, Inc.). Three measurements consisting of 3 scans of 5 s each were acquired in backscatter (173°) mode. The instrument automatically determined the best attenuation factor and measurement position. The mean count rate was ~200 kcps.

Zeta Potential

Dispersions of graphenic materials with a concentration of 50 ug/mL in water were buffered to pH 9 and 5 using NaOH and HCl, then loaded into Malvern disposable folded capillary cells (DTS1070). Zeta potentials were measured using the same instrument and software as DLS. Three measurements were acquired using the optimal scanning parameters of the instrument (ranging from 10-100 scans per measurement).

Bulk Density and Porosity

The dimensions of the 3D constructs (cylindrical pellets) were measured using Ultra-Cal V electronic calipers (Fowler). Porosity was calculated using the theoretical density of graphite (2.26 g cm^{-3}).

Bulk Conductivity

A Signatone SP4 (Gilroy, CA) four-point probe was used to assess the electrical properties of the graphenic pellets. 21V was applied across the surface of the sample, and the resistance was detected using a Keithley 2400 Sourcemeter (Cleveland, OH). Twenty resistance measurements were made per sample to ensure accuracy. Given the finite sample thickness and diameter, the resistivity was corrected using standard literature procedure.[5] Resistivity measurements were converted to conductivity by taking the inverse.

Dynamic Mechanical Analysis (DMA)

A Discovery Hybrid rheometer (TA Instruments, New Castle, DE) was used to perform DMA. After applying a 1 N pre-stress, axial compression was measured at room temperature at a strain rate of 0.1% at 1Hz. The resulting data was analyzed using TRIOS software.

Universal Testing

Universal compressive testing was performed on an Instron 4469 with a 50 kN load cell (Instron, Norwood, MA). Pelleted samples were compressed until failure at a strain rate of 0.1 s^{-1}. Raw data was corrected used toe compensation according to ASTM D638.

Ultraviolet/Visible Spectroscopy

UV-Vis spectra of layer-by-layer coated glass slides were acquired with a Varian Cary 5000 spectrophotometer.

C. Calculations

Scheme S1. Calculation of Atomic Percent Peptide on Pep-G Surface

Since XPS is a surface characterization technique, the percent nitrogen in the Pep-G ($\%N_{conjugate}$) in conjunction with the theoretical percent nitrogen in the peptide ($\%N_{peptide}$) are used to calculate the percent of total atoms on the Pep-G surface that can be attributed to peptide (%Peptide). This metric gives a general idea of the functionalization density of these materials.

To calculate theoretical %N from the peptide for Lysine(Z):

$$\left\{\begin{array}{c} C_{peptide} = 6 + (14 \times DP) \\ O_{peptide} = 3 \times DP \\ N_{peptide} = 1 + (2 \times DP) \\ C_{peptide} + O_{peptide} + N_{peptide} = Atoms_{peptide} \end{array}\right\} \rightarrow \%N_{peptide} = \frac{N_{peptide}}{Atoms_{peptide}} \times 100\%$$

To calculate theoretical %N from the peptide for Glutamate(Bzl):

$$\left\{\begin{array}{c} C_{peptide} = 6 + (12 \times DP) \\ O_{peptide} = 3 \times DP \\ N_{peptide} = 1 + DP \\ C_{peptide} + O_{peptide} + N_{peptide} = Atoms_{peptide} \end{array}\right\} \rightarrow \%N_{peptide} = \frac{N_{peptide}}{Atoms_{peptide}} \times 100\%$$

$$\%N_{conjugate} = \%Peptide(\%N_{peptide}) + \%CG(\%N_{CG})$$

$$\%N_{CG} = 0; therefore, \quad \%Peptide = \frac{\%N_{conjugate}}{\%N_{peptide}}$$

$\%N_{conjugate}$ was determined by an average from XPS survey scans run in triplicate. DP (degree of polymerization) of peptides was determined by ^{1}H NMR.

C. Characterization

Figure S1. Dynamic Light Scattering (DLS) of graphenic starting materials, GO and CG. Z-average particle sizes were found to be 2.4 ± 1.4 μm and 2.7 ± 1.2 μm for GO and CG, respectively.

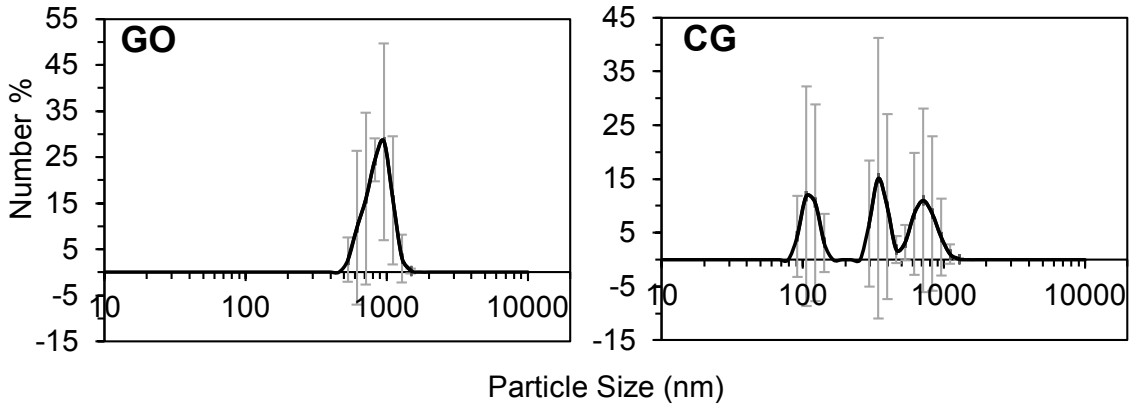

Figure S2. A) Methacrylate-terminated p(Lys-Z) was subjected to coupling conditions with CG, resulting in no reaction between the two materials. **B)** The resulting graphenic material was washed using the same procedure described in the methods; the wash solvents were evaporated, weighed, and analyzed. **C)** The graphenic material showed a small amount of nitrogen in the XPS survey scans, indicating that some peptide remained adsorbed to the graphenic material after washing. Nevertheless, TGA indicated that very little peptide was adsorbed to the graphenic product, as covalent or noncovalent peptide coupling would have resulted in an additional degradation event between 215-315 ˚C compared to CG. **D)** The reaction supernatant contained a yellow residue with trace graphenic particles. ^{1}H NMR (500 MHz, DMSO-d_6) of the reaction supernatant looked identical to the ^{1}H NMR spectra of the peptide prior to the control reaction, indicating that the unbound peptide was primarily separated from the graphenic product via filtration.

(A) Synthetic Scheme

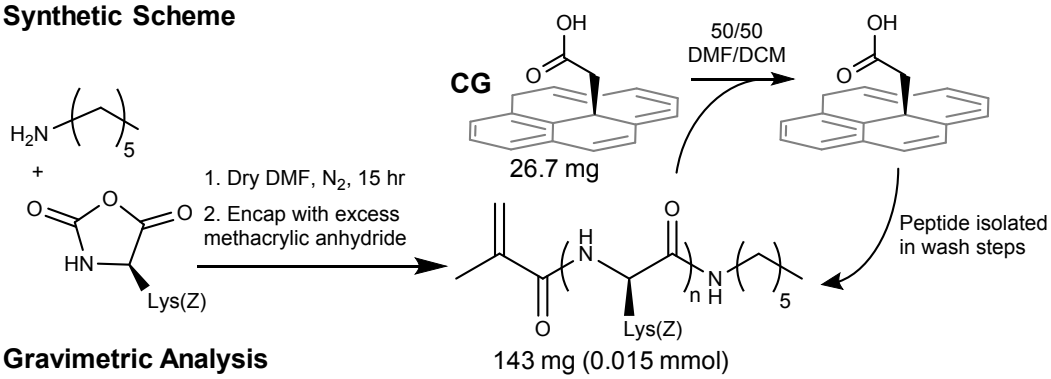

(B) Gravimetric Analysis

Component	Dry Mass	Notes
Graphenic product	31.1 mg	Characterized by XPS and TGA; determined to be primarily CG with minimal adsorbed peptide
Reaction supernatant + DMF washes	144.8 mg	Characterized by ^{1}H NMR; determined to be neat peptide with trace graphenic particles
DCM washes	17.9 mg	Contained trace graphenic particles
Acetone washes	2.5 mg	Contained trace graphenic particles
H_2O washes	1.3 mg	Contained trace graphenic particles

(C) Analysis of Graphenic Product

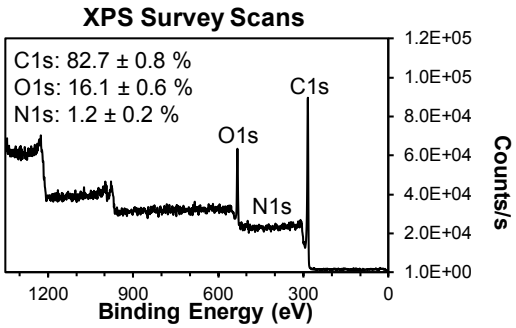

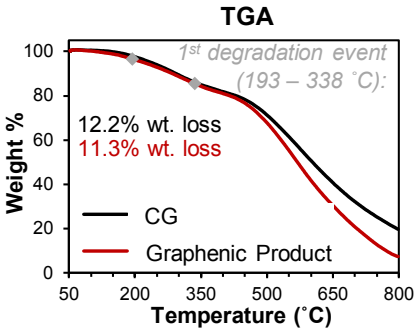

(D) Analysis of Reaction Supernatant

Evaporated reaction supernatant

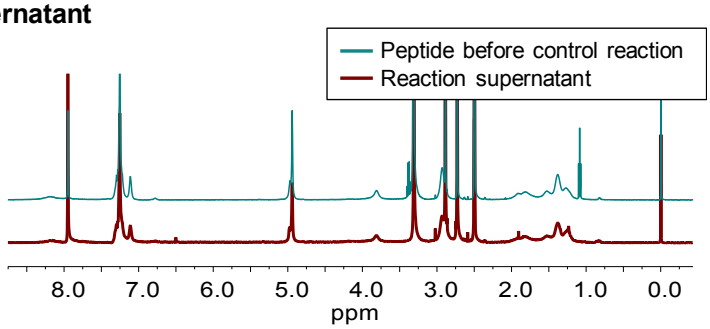

Figure S3. GPC was used to define the dispersity of the peptides, and ^{1}H NMR was used to define the molecular weight by end group analysis. These analyses were performed prior to conjugating the peptides to CG. Note that DP is degree of polymerization, and Đ represents polydispersity index.

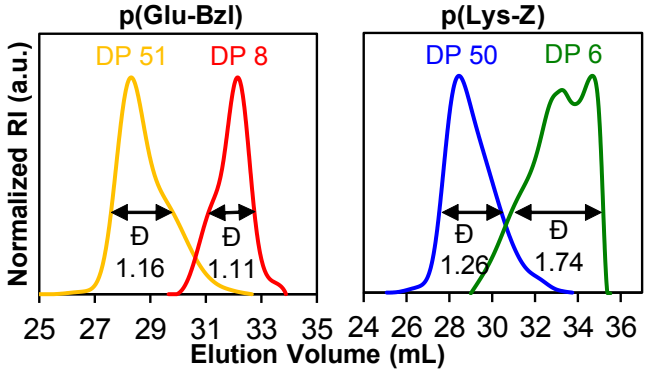

Table S2. Molecular weight values of peptides are obtained from ^{1}H NMR and GPC (DMF, calibrated with PMMA). GPC predicts a higher M_n for p(Glu-Bzl) and lower M_n for p(Lys-Z) when compared to M_n's calculated from NMR. This trend is supported by literature[6] and can be attributed to differences hydrodynamic volume compared to the standardization polymer, polymethylmethacrylate.

Polymer	M_n by NMR (kDa)	M_n by GPC (kDa)	M_w by GPC (kDa)
$p(Glu\text{-}Bzl)_{short}$	1.85	3.62	4.02
$p(Glu\text{-}Bzl)_{long}$	11.28	13.47	15.56
$p(Lys\text{-}Z)_{short}$	1.67	1.44	2.51
$p(Lys\text{-}Z)_{long}$	13.22	10.63	13.37

Figure S4. Fourier Transform Infrared (FTIR) Spectroscopy shows characteristic amide peaks at 1653 and 1544 cm^{-1} in protected Pep-G (red, yellow, green, and blue) confirming the presence of peptide in these conjugates. These amide peaks are not present in the parent material, GO (grey), but native functional groups in CG show peaks that overlap with the amide regions.

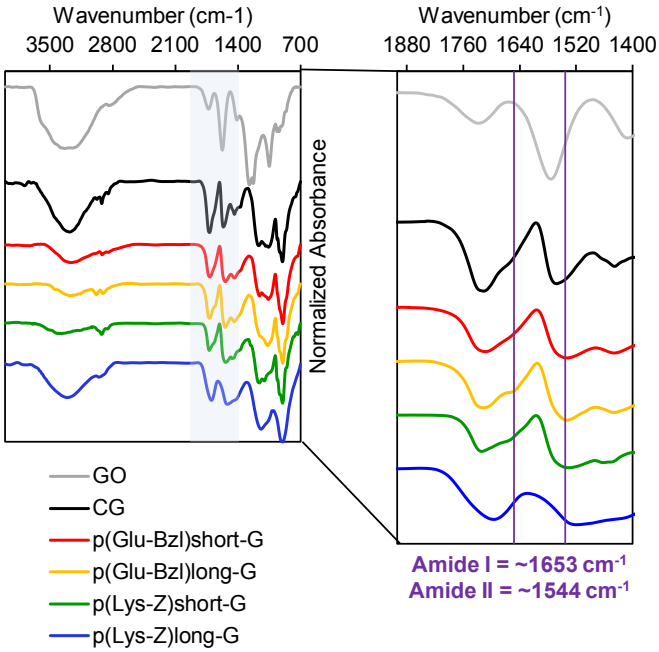

Figure S5. Thermogravimetric analysis (TGA) shows a clear difference in thermal degradation profile after protected peptide conjugation to CG.

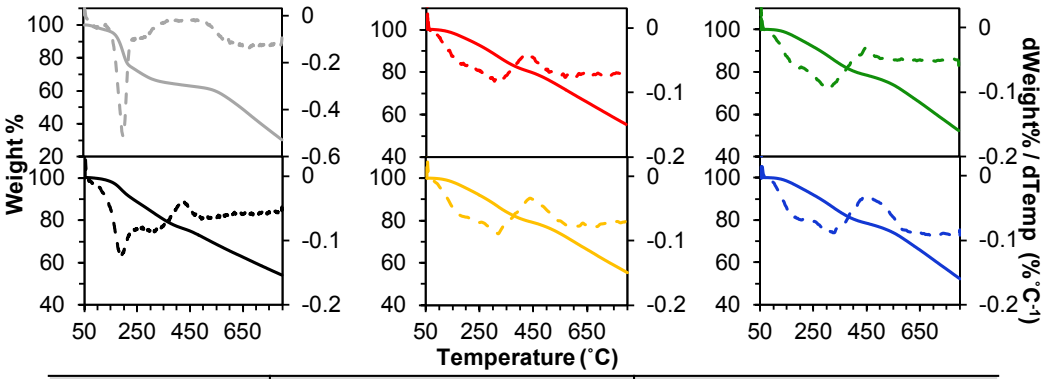

Material	Degradation I			Degradation II		
	To (˚C)	Tp (˚C)	% Wt. Loss	To (˚C)	Tp (˚C)	% Wt. Loss
GO	175.2	198.6	15.44	220.7	247.7	8.65
CG	157.2	188.8	5.86	213.0	315.5	13.41
Glu(Bzl)short-G	134.5	197.7	4.24	216.1	299.1	11.29
Glu(Bzl)long-G	135.2	203.6	5.04	223.3	322.6	12.43
Lys(Z)short-G	136.5	179.1	4.48	217.6	304.4	12.95
Lys(Z)long-G	138.3	186.3	4.77	216.7	317.6	13.21

Figure S6. Deprotection of p(Lys-Z)$_{short}$-G to give p(Lys)$_{short}$-G **(A)** and p(Glu-Bzl)$_{short}$-G to give p(Glu)$_{short}$-G **(B)** is indicated by deconvolution of N1s and O1s XPS spectra, respectively. Percentages of each nitrogen or oxygen-containing functional group within the peptide-graphene conjugates demonstrate deprotection of peptides.

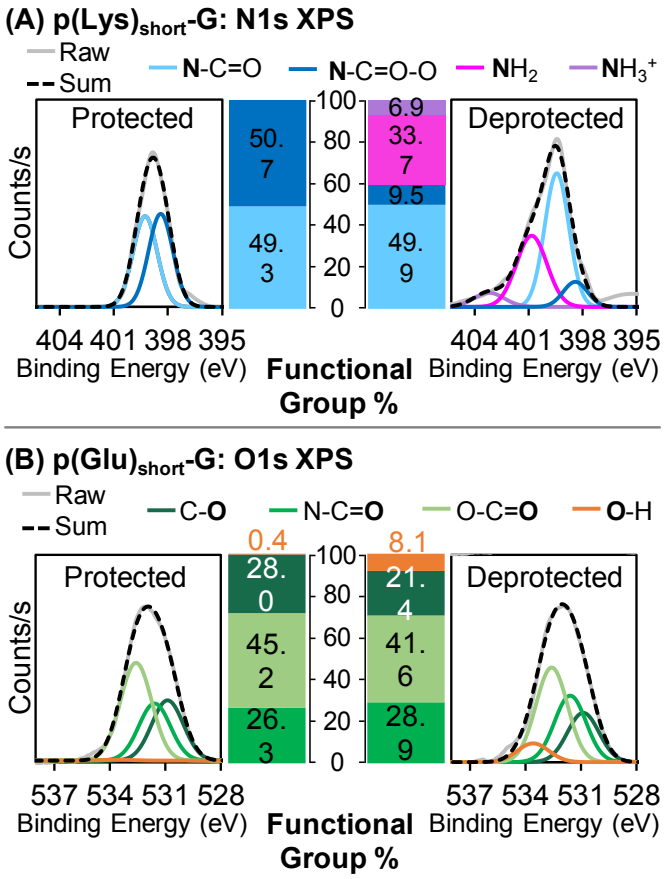

Figure S7. XRD demonstrates that the graphenic materials are ordered from largest to smallest intergallery spacing in the following arrangement: GO, CG, protected Pep-G conjugates, then deprotected Pep-G conjugates. Note that the solid green, blue, red, and yellow lines represent protected Pep-Gs, while the dashed spectra represent deprotected Pep-Gs.

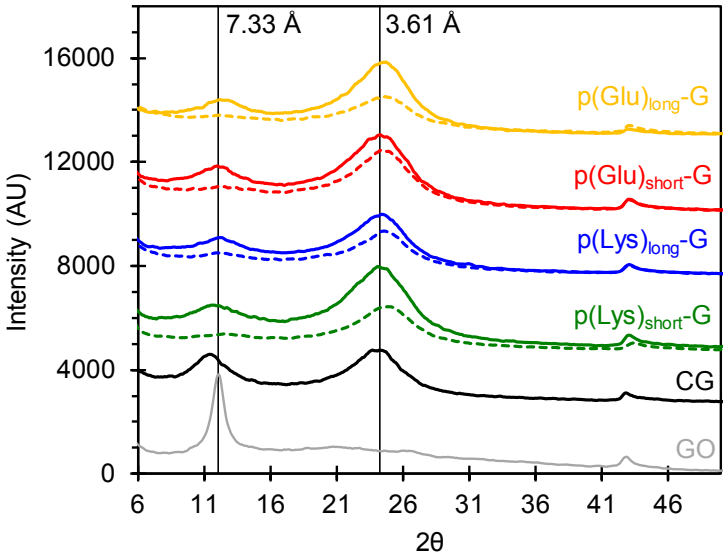

When GO is reacted to form CG, the XRD spectra changes in two primary ways: 1) an increase in sheet spacing from 7.33 to 7.81 Å is seen because some CG sheets are more exfoliated than GO; and 2) a peak at 3.61 Å appears because CG is more chemically reduced than GO – restored conjugation in CG provides stronger π-π interactions between sheets, bringing them closer together. When peptide is conjugated to CG to yield a Pep-G, the peak at 7.81 Å becomes smaller (both in magnitude and intensity), and the peak at 3.61 Å becomes the dominant peak. This indicates that peptide conjugation leads to generally smaller sheet spacing compared to neat CG. Deprotection of the peptide on Pep-G leads to a significant decrease in the peak at 7.33 Å, demonstrating that sheet spacing becomes homogenously small (3.61 Å). These trends in sheet spacing are consistent with the unique trends seen in the conductivity of the Pep-G and parent materials: materials with smaller sheet spacing exhibit greater conductivity.

Figure S8. A) Density of 3D graphenic constructs was evaluated based on mass and dimensions of pressed pellets. Axial compressive DMA demonstrates that all pellets are more elastic than viscous, as the storage modulus, E', **(B)** is greater than the loss modulus, E'', **(C)**. Stress-strain curves in compression **(D)** were used to calculate toughness (**E**).

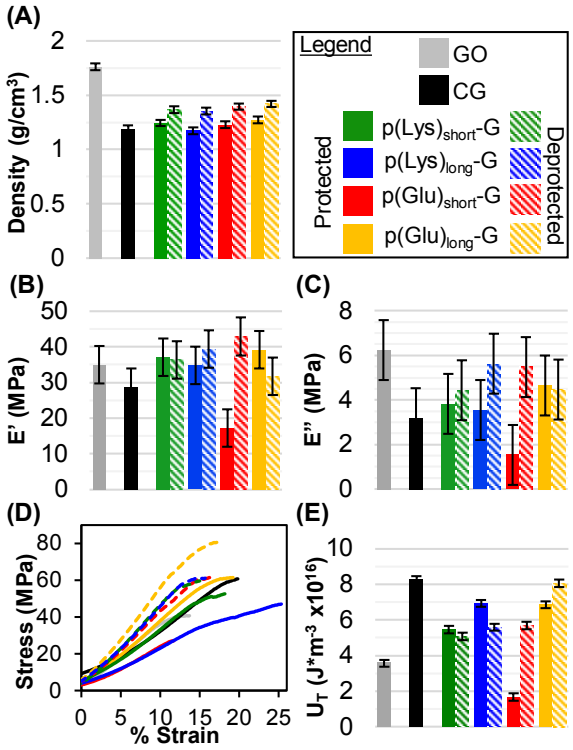

Figure S9. A pellet of noncovalently blended p(Glu-Bzl) + CG was compressed to failure, giving a stress-strain curve. This curve was used to calculate ultimate compressive strength (UCS), Young's Modulus (E), and toughness. The mechanical properties of the noncovalent peptide + CG blend are far lower than those of the covalent Pep-G conjugates and their parent materials (GO and CG) – they could not be visualized on the same stress scale.

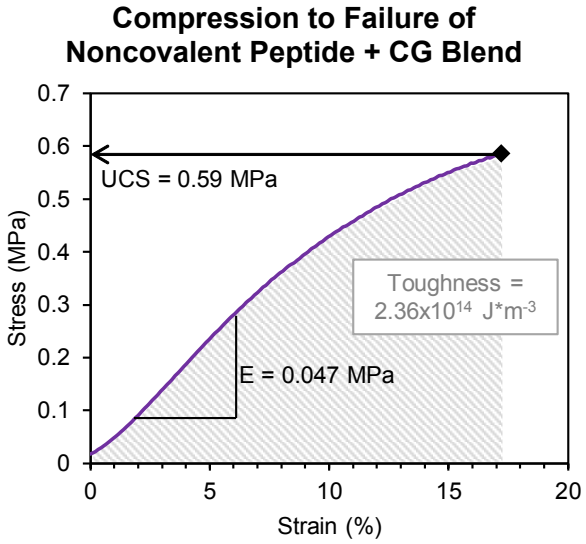

D. Methods

Formulation of Noncovalent Peptide + CG Blend

To create a noncovalent blend of peptide with CG, 0.016 mmol of p(Glu-Bzl) was dissolved in approximately 2 mL of DMF. Then, 0.3827 g of CG was added to the solution and dispersed by 5 min of sonication. The peptide was coprecipitated with the CG by adding 40 mL of cold diethyl ether. The mixture was centrifuged at 2160×*g* for 10 min (Z 366, HERMLE Labortechnik GmbH, Wehingen, Germany) and the supernatant discarded. The resulting material was dried under vacuum overnight. The noncovalent Pep+G material was noticeably doughier and more malleable than the covalent Pep-Gs, which have a powdered texture similar to CG and GO. The blend was pressed into a pellet as described in the main text and used for conductivity and mechanical testing.

Cell Culture

Human adipose-derived mesenchymal stem cells (hMSCs) were purchased from ThermoFisher Scientific (#R7788115) and cultured in complete MesenPRO RS™ Medium (ThermoFisher Scientific, #12746012) supplemented with 200 mM L–glutamine (ThermoFisher Scientific, #25030081) diluted to 2 mM and 10 000 U/mL penicillin-streptomycin diluted to 100 U/mL (ThermoFisher Scientific, #15140122). MesenPRO RS™ Medium is a reduced serum media specially formulated to support the growth of hMSCs while preserving their multipotency for multiple passages. For detaching cells during routine subculture, TrypLE™ Express without phenol red (ThermoFisher Scientific, #12604013) was used due to its enhanced purity and specificity that decreases damage to cells compared to trypsin. All stem-cell reagents were free from phenol red since it has been reported that phenol red affects differentiation of hMSCs.[7]

RAW 264.7 murine macrophages were cultured in Dulbecco's Modified Eagle Medium with concentrations of 4,500 mg/L for D–glucose, 584 mg/L of L–glutamine, and 100 mg/L sodium pyruvate (ThermoFisher Scientific, #11995065), supplemented at 10% v/v with fetal bovine serum (ThermoFisher Scientific, #26140079) and 1% v/v penicillin-streptomycin. NIH-3T3 murine fibroblasts were cultured in the same basal medium as RAW 264.7 macrophages but supplemented at 10% v/v with calf serum (ThermoFisher Scientific, #16010159) and 1% v/v penicillin-streptomycin.

All cells were cultured in filter cap 25 cm^2 flasks (Greiner Bio-One CELLSTAR®, #690175) for routine subculture and 96-well plates (Greiner Bio-One CELLSTAR®, #655180) for experiments at 37 °C with a humidified atmosphere at 5% CO_2.

Cytocompatibility Assay

Graphenic materials were directly dispersed in complete cell culture media. Powders were weighed out into centrifuge tubes and sterilized by exposure to the 250 nm ultraviolet light of the biosafety cabinet for 10 min. Then, the powders were diluted in complete cell culture media to a concentration of 1000 μg/mL. Since the graphenic materials remained flocculated after the

addition of media, the mixtures were bath sonicated for ~1 min (240 W, 42 kHz, ultrasonic cleaner, Kendal) to disperse the flocculants. From these stock solutions, 10× serial dilutions were prepared (100 and 10 μg/mL). For the negative control, nothing was added into the media. For the positive control, bioreagent grade dimethyl sulfoxide (Alfa Aesar, #J66650) was administered at 10% v/v. For all experimental conditions, enough suspension was prepared for technical triples and was used immediately.

Cells were subcultured and seeded in 96-well plates at 20% confluency from the same stock suspension of cells. After ~3 h, the cells were well-adhered. Then, the media was aspirated, and the cells exposed to media spiked with the experimental samples described above.

After 2 days, the cells were assayed for vitality and death. The media was aspirated and the cells were washed twice with phosphate buffered saline (PBS, ThermoFisher Scientific, #10010049). The PBS was aspirated, and the cells were exposed to 75 μL per well of staining solution for 10 min at 37 °C. The staining solution consisted of 20 mM Hoechst 33342 (ThermoFisher Scientific, #62249) diluted to 20 μM, 1 mM Calcein-AM (PromoKine, #PK–CA707–80011–2) diluted to 2.5 μM, and 2 μg/mL propidium iodide (Alfa Aesar, #J66584) diluted to 2 μM in PBS.

A TECAN Spark® microplate reader with SparkControl™ v2.2 software was used to quantify fluorescence: Hoechst 33342 excitation 350/20 nm, emission 450/20 nm; Calcein-AM excitation 485/15 nm, emission 525/15 nm; and propidium iodide excitation 530/20 nm, emission 620/20 nm. Absorbance spectra were also acquired (350:10:700 nm). Immediately following, the cells were rapidly imaged using EVOS® FL Auto Cell Imaging System (ThermoFisher Scientific) with a 20×, 0.40 numerical aperture objective. Fluorescence images were acquired using the DAPI light cube (357/44 Ex; 447/60 Em), GFP light cube (470/22 Ex; 510/42 Em), and the RFP light cube (531/40 Ex; 593/40 Em); and phase contrast images were also acquired at the same imaging parameters across all samples.

Cytocompatibility Data Analysis

Since high concentrations of graphenic materials can interfere with fluorescence assays, we acquired fluorescence intensity and absorbance of a stock staining solution (as described above) spiked with varying concentrations of GO. This calibration curve of fluorescence quenching versus absorbance was used to adjust the as-acquired Calcein-AM fluorescence intensities from the cell experiments. Finally, the vitality bars are Calcein-AM mean fluorescence intensity, the error bars are standard error, and $n = 3$.

The graphenic interference at 1 mg/mL was too severe to result in accurate plate reader intensity data for the Hoechst 33342 and propidium iodide channels. Thus, their fluorescence images were analyzed to determine percent dying cells. MATLAB (MathWorks®) was used to automatically detect and count elliptical objects that correspond to individual cell nuclei. Manual verification was performed, and this was especially important for some images which had lower signal-to-noise ratios or other regions of non-specific intensity. For the RAW 264.7 macrophages, there

were so many cells that their nuclei were too close together to accurately automatically segment separate elliptical objects. Thus, their image intensities were used to determine percent dead cells, relating the intensity proportions to the known percent dead cells of the no treatment control. For hMSCs and NIH-3T3 fibroblasts, total cells per sample were calculated from the number of all identified nuclei from the Hoechst 33342 images, and total dying cells per sample were calculated from the number of all identified nuclei from the propidium iodide images. Then, the percent dying cells was calculated and reported. The error bars are the standard error calculated from the standard deviation, σ, of a proportion, p, of sample size, n:

$$D. \quad \sigma = \sqrt{p(1-p)/n}$$

Note that analyzing the proportion of dead-to-live cell data as a whole sample rather than averaging proportions determined on an image-by-image basis provides a more accurate representation of the population. At least six images were analyzed for each channel of each sample, resulting in at least 50 cells per sample (322 ± 28, mean ± standard error) being analyzed.

Electrical stimulation

We designed an electrical circuit to provide pulsed DC stimulation of physiologically relevant magnitude using a 555 timer IC with an output of 5 mV, pulse width modulation of 60 Hz, and duty cycle of 62.9% (Figure S8 A–C). To provide electrical stimulation to the scaffold, the scaffold was mounted on top of copper tape, and bioinert and cytocompatible high vacuum grease (Dow Corning®, #1597418) was used to electrically isolate the cell culture media (Figure S8 D,E). Based on the conductivities of pellets of CG and $p(Lys)_{long}$-G, the corresponding cross-pellet resistances are ~1000 and ~50 Ω, respectively. For a voltage potential of 5 mV, the cross pellet current would be ~5 and ~100 μA, respectively, and the cross pellet current per area would be ~50 and ~1000 μA cm^{-2}. However, the contacts are not on opposite sides of the pellet; thus, the voltage potential and current at the cell growth surface will be lower.

PC12 cells were cultured in RPMI 1640 Medium, ATCC modification (ThermoFisher, #A1049101) supplemented with 10% v/v fetal bovine serum (ThermoFisher, #26140079), 5% v/v heat inactivated horse serum (ThermoFisher, #26050088), and 1% v/v 10000 U mL^{-1} penicillin-streptomycin (ThermoFisher, #15140122). For subculture of PC12 cells in 25 cm^2 tissue culture flasks (Greiner Bio-One CELLSTAR®, #690175), conditioned media was aspirated and replaced with fresh media (5 mL). Then, the cells were dislodged using a cell scraper, followed by trituration using a sterile, 22-gauge hypodermic needle (AIR-TITE, #N22312). The resulting cell suspension was diluted 1:5 and seeded into fresh flasks or onto pellets of graphenic materials, described below.

The cellular testing chamber was sterilized by exposure to the 250 nm ultraviolet light of the biosafety cabinet for 10 min. After sterilization, PC12 cells were seeded onto the surface of the pellet, and the inner test chamber was flooded with media (~300 μL). The circuit was connected to the battery power source, and the whole setup was placed into a humidified incubator maintained at 37 °C and 5% CO_2 for 2 days.

Fixation and Sub-cellular Compartment Imaging

After two days of culture on the electrically stimulated pellets, Hoechst 33342 and MitoTracker™ Red CMXRos (ThermoFisher, #M7512) were directly added to the media, being diluted to a final concentration of 5 μM and 1 μM, respectively. After 30 min, the circuit power source was disconnected, the media gently aspirated, the cells gently washed with PBS, and the cells exposed to 3.7% v/v formaldehyde in PBS for 10 min. The formaldehyde was aspirated, the cells washed with PBS, and cell membranes were permeabilized with 0.2% v/v Triton X-100 in PBS for 5 min. The surfactant solution was aspirated, the cells washed with PBS, and then exposed to Acti–stain™ 488 phalloidin (Cytoskeleton, Inc., #PHDG1) at 100 nM for 1 h. The filamentous actin (F-actin) staining solution was aspirated, and the cells were washed with and maintained in PBS.

The PC12 cells cultured on the pellets were imaged using an inverted EVOS® FL Auto Cell Imaging System. Since the cells were cultured on top of the pellets, a #1.5 coverslip was suspended on the microscope stage, a 10 μL drop of PBS was added, and the pellet was inverted and placed (cell side down) on the coverslip. Then, whole-pellet images were acquired by concatenating numerous fields of view acquired using a 10×, 0.30 numerical aperture objective using EVOS® FL Auto software. High-resolution images were acquired using an oil-immersion, 1.4 numerical aperture, 100× objective. Overlay images were prepared in ImageJ (National Institutes of Health).

Figure S10. Overview of the electrical circuit design and cellular testing chamber. **(A)** Circuit diagram. **(B)** Optical image of the circuit, on top of a 9 V battery power source. **(C)** Image of the oscilloscope output of the circuit. **(D)** Schematic depiction of the cellular testing chamber. The pulsed circuit output is conducted through the copper tape and into and across the graphenic pellet. The bioinert, cytocompatible vacuum grease ensures current is not passed into the liquid cell culture media. **(E)** Optical image of a pellet attached to the circuit in the testing chamber.

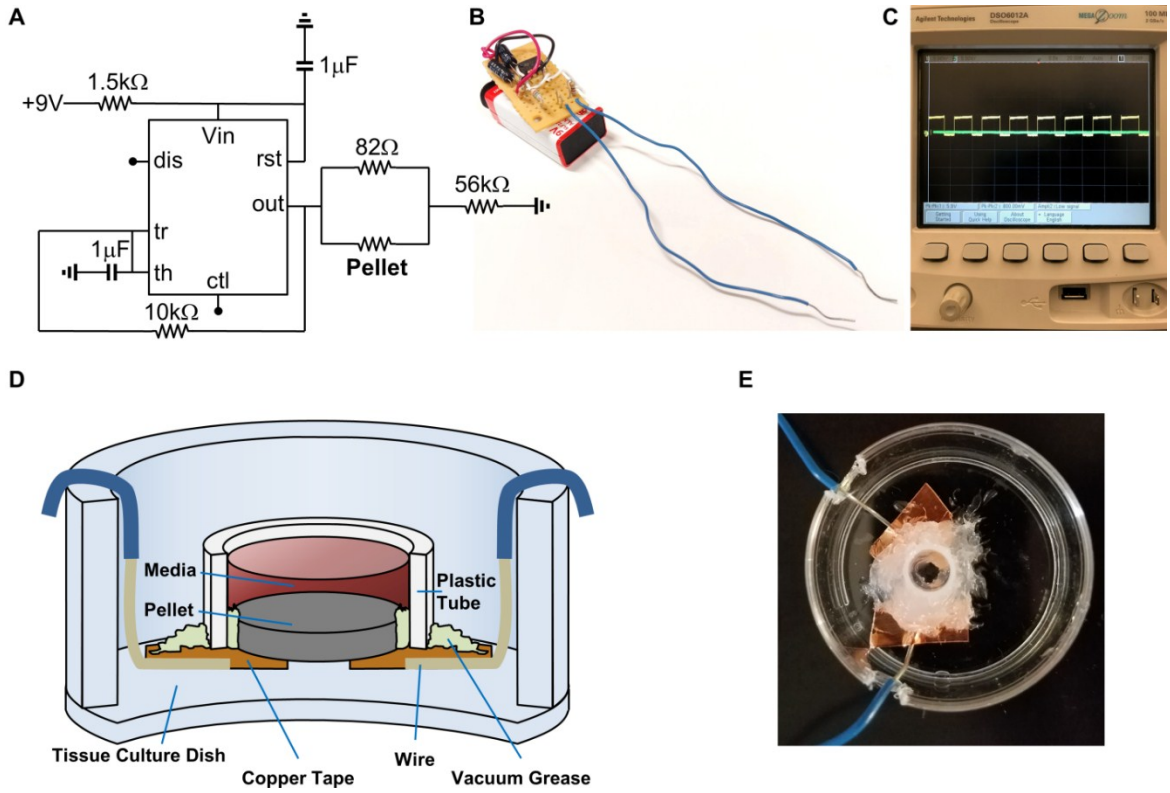

E. References

(1) Wojdyr, M. Fityk: A General-Purpose Peak Fitting Program. *J. Appl. Crystallogr.* **2010**, *43* (5), 1126–1128. https://doi.org/10.1107/S0021889810030499.

(2) Wagner, C. D. *Handbook of X-Ray Photoelectron Spectroscopy: A Reference Book of Standard Data for Use in X-Ray Photoelectron Spectroscopy*; Perkin-Elmer, 1979.

(3) Yu, B.; Wang, X.; Qian, X.; Xing, W.; Yang, H.; Ma, L.; Lin, Y.; Jiang, S.; Song, L.; Hu, Y.; et al. Functionalized Graphene Oxide/Phosphoramide Oligomer Hybrids Flame Retardant Prepared via in Situ Polymerization for Improving the Fire Safety of Polypropylene. *RSC Adv.* **2014**, *4* (60), 31782–31794. https://doi.org/10.1039/C3RA45945D.

(4) Iqbal, M. Z.; Katsiotis, M. S.; Alhassan, S. M.; Liberatore, M. W.; Abdala, A. A. Effect of Solvent on the Uncatalyzed Synthesis of Aminosilane-Functionalized Graphene. *RSC Adv.* **2014**, *4* (13), 6830–6839. https://doi.org/10.1039/C3RA46586A.

(5) Smits, F. M. Measurement of Sheet Resistivities with the Four-Point Probe. *Bell Syst. Tech. J.* **1958**, *37* (3), 711–718. https://doi.org/10.1002/j.1538-7305.1958.tb03883.x.

(6) Huesmann, D.; Birke, A.; Klinker, K.; Türk, S.; Räder, H. J.; Barz, M. Revisiting Secondary Structures in NCA Polymerization: Influences on the Analysis of Protected Polylysines. *Macromolecules* **2014**, *47* (3), 928–936. https://doi.org/10.1021/ma5000392.

(7) Lysdahl, H.; Baatrup, A.; Nielsen, A. B.; Foldager, C. B.; Bünger, C. Phenol Red Inhibits Chondrogenic Differentiation and Affects Osteogenic Differentiation of Human Mesenchymal Stem Cells in Vitro. *Stem Cell Rev. Rep.* **2013**, *9* (2), 132–139. https://doi.org/10.1007/s12015-012-9417-0.